Blueprint for efficient nuclear spin characterization with color centers

Majid Zahedian,[1,2] Vadim Vorobyov,[1,*] and Jörg Wrachtrup[1,3]
[1]*3rd Physical Institute University of Stuttgart, 70569 Stuttgart, Germany*
[2]*Institute of Quantum Electronics, ETH Zürich, 8093 Zürich, Switzerland*
[3]*Max Planck Institute for Solid State Research, 70569 Stuttgart, Germany*

(Received 27 March 2024; revised 3 June 2024; accepted 7 June 2024; published 26 June 2024)

Nuclear spins in solids offer a promising avenue for developing scalable quantum hardware. Leveraging nearby single-color centers, these spins can be efficiently addressed at the single-site level through spin resonance. However, characterizing individual nuclear spins is quite cumbersome since the characterization protocols may differ depending on the strength of the hyperfine coupling, necessitating tailored approaches and experimental conditions. While modified electron spin Hahn echoes like Carr-Purcell-Meiboom-Gill (CPMG) and phase cycled CPMG (XY8) pulse sequences are commonly employed, they encounter significant limitations in scenarios involving spin-1/2 systems, strongly coupled spins, or nuclear spin baths comprising distinct isotopes. Here, we present a more straightforward approach for determining the hyperfine interactions among each nuclear spin and the electron spin. This method holds promise across diverse platforms, especially for emerging $S = 1/2$ group IV defects in diamond (e.g., SiV, GeV, SnV, PbV) and silicon (T center, P donors). We provide a theoretical framework and adapt it for color centers exhibiting various spins. Through simulations conducted on nuclear spin clusters, we evaluate different protocols and compare their performance using the Fisher information matrix and Cramér-Rao bounds.

DOI: 10.1103/PhysRevB.109.214111

I. INTRODUCTION AND BACKGROUND

Optically active defects in solids, known as color centers, have been utilized in various quantum applications [1], including quantum networks [2], quantum sensing [3,4], and quantum registers [5–9]. Each center contains an electron spin that can be directly controlled using microwaves, and it can be initialized and read out through optical excitation. The potential hyperfine interactions with a bath of numerous nuclear spins are crucial for diverse applications, as they offer long-lived quantum memories and enable the creation of an optically accessible nuclear spin qubit register. To implement efficient quantum control for these memories, it is imperative to have precise knowledge of the full Hamiltonian governing the register [10,11]. However, characterizing the hyperfine coupling of nuclear spins can be both challenging and time-consuming [12,13]. Traditionally, nuclear spin characterization is accomplished through optically detected magnetic resonance [7,14], but the spectroscopic resolution is constrained by the $1/T_2^*$ of the electron spin. To overcome this limitation, Hahn-echo-type sequences have been employed to refocus the electron spin and extend its coherence time [15], thereby improving the resolution to $1/T_2$. This method can be applied to defects with a specific configuration of nuclear spins, particularly those with a certain relation to the magnetic field and the coupling of the nuclear spins, such as weakly coupled nuclear spins. Also, the protocols can be applied only to electron spins with a specific spin multiplicity. Depending on the applied protocol for the nuclear spin characterization, the number of identifiable nuclear spins can be different. Electron spin echo envelope modulation (ESEEM) types of sequences allow access to the highest number of nuclear spins, as the spectroscopy resolution is limited to the longitudinal relaxation time T_1 of the system (see Fig. 1) [16,17]. In particular, we consider the following common examples of nuclear spin registers that are ubiquitous in applications. First, we consider the NV-like case with $S = 1$ and weakly coupled nuclear spins, operating at high magnetic fields where $\gamma_n B \gg A_{zx}$, which has been extensively studied [12,18,19]. The capability to observe narrow peaks with analytically predictable positions and contrasts enables the solution of the inverse problem concerning the characterization of the coupling between nuclear and electron spins. The second case [as depicted in Fig. 1(b)] corresponds to a scenario similar to the first, but with the presence of a strongly coupled nuclear spin, which obstructs the observation of weakly coupled nuclear spins. This case is particularly relevant in situations where, in addition to the weakly coupled register, a strongly coupled nuclear spin is utilized, for instance, for repetitive enhancement of readout [20]. This enhancement is achieved by exploiting the strongly coupled ancilla, which is discernible in electron spin resonance spectra. The third case [Fig. 1(c)] pertains to the $S = 1/2$ scenario, where the lack of offset in the average evolution of the nuclear spin results in its dynamics weakly depending on A_{zz} and only second-order dependence on A_{zx}. Consequently, this leads to a limited ability to distinguish between multiple nuclear spins and a lack of individual addressability of nuclear spins. Last, in the case of other material host platforms, a bispecies nuclear spin bath may be observed, where resonance peaks corresponding to different Larmor frequencies of different species further complicate the

*Contact author: v.vorobyov@pi3.uni-stuttgart.de

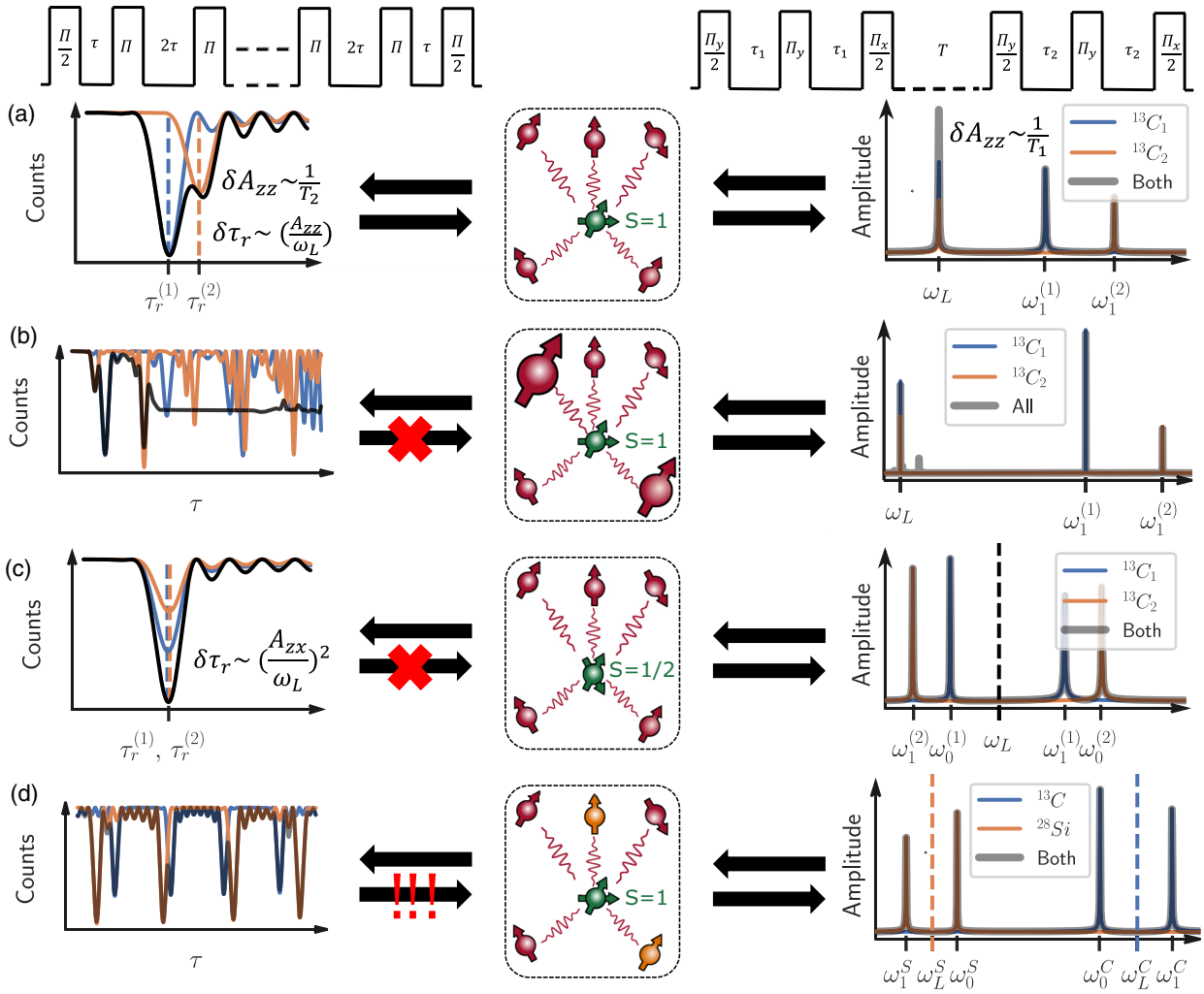

FIG. 1. Comparing DD and five-pulse ESEEM as two nuclear spin characterization methods in different systems. (a) Electron spin-1 system: In the DD signal, each nuclear spin exhibits a distinct resonance time up to the first order of A_{zz}; the accuracy of the obtained hyperfine interaction is limited to T_2 of the electron spin. In the Fourier transform of the ESEEM signal, the two resonance frequencies of each spin are present; the accuracy of the obtained hyperfine interaction is limited to T_1 of the electron spin. (b) Electron spin-1 system with two strongly coupled nuclear spins and many weakly coupled spins: No resonance time is detectable since the required condition for DD ($\omega_L \gg A_{zz}, A_{zx}$) does not hold. However, resonant frequencies are still obtainable in the ESEEM signal. (c) Electron spin-1/2 system: Nuclear spins have more or less the same resonance time because it depends on the second order of hyperfine coupling. However, the resonant frequency of each spin is distinguishable in the ESEEM signal. (d) System containing two different nuclear spin species: Two nuclear spin baths can interfere in the DD signal, making the signal analysis more challenging. However, the species can be inferred from the ESEEM signal since species have different Larmor frequencies.

reconstruction of the Hamiltonian. For unambiguous reconstruction of the interactions, additional measurements, such as those at different magnetic field strengths, would be required. While double-resonance methods [5,21] hold large promise for nuclear spin spectroscopy, they require additional experimental hardware and often are not available. Thus, in this work, we investigate the limits of electron spin driven schemes, in particular correlation-type sequences, which could serve as a general framework and hold promise for the reconstruction of the interactions in all of the aforementioned cases.

II. RESULTS

We consider a central spin system of *noninteracting* nuclear spins $I = 1/2$ coupled to a central electron spin $\boldsymbol{S}$. The central electron spin is manipulated resonantly with microwave pulses, which transfer the population between the two sublevels denoted as $m_s = s_0$ and $m_s = s_1$. These two spin sublevels are separated due to the Zeeman effect and/or zero-field splitting, forming a two-level subsystem with an energy splitting of ω_a. The Hamiltonian of the system in the secular approximation and in the rotating frame of the applied microwave ω_{mw} can be written as (see the derivation in Appendix B)

$$H = \Delta S_z + \sum_k \left(\omega_L^{(k)} + A_{zz}^{(k)} S_z\right) I_z^{(k)} + A_{zx}^{(k)} S_z I_x^{(k)}, \qquad (1)$$

where $\Delta = \omega_a - \omega_{mw}$ is the detuning; $\omega_L^{(k)} = \gamma_n^{(k)} B$ is the nuclear Rabi frequency, with $\gamma_n^{(k)}$ being the nuclear spin

gyromagnetic ratio and B being the external magnetic field; and A_{zz} and A_{zx} are the parallel and perpendicular secular components of the hyperfine tensor, respectively. The Hamiltonian is diagonal in the electron spin subspace; thus, the Hamiltonian for the nuclear spins can be rewritten in the electron spin subdomains s_i ($i = 0, 1$). The nuclear spin Hamiltonian can be solved for eigenenergies, which determine the precession frequencies of $\omega_i = \sqrt{(\omega_L + s_i A_{zz})^2 + (s_i A_{zx})^2}$, $i = 0, 1$, along the eigenvector axes $\vec{n}_i = (\frac{s_i A_{zx}}{\omega_i}, 0, \frac{\omega_L + s_i A_{zz}}{\omega_i})$. It is assumed that the pulse duration t_p is short enough ($\omega_L t_p \ll 1$) that the nuclear spin dynamics during this time is negligible. For completeness, we start our analysis with the simplest characterization sequence, which is the electron spin Ramsey sequence (free induction decay of the electron). The Ramsey signal can be obtained as follows:

$$\langle \sigma_z \rangle_{\mathrm{Ram}} = \cos(\Delta\tau) \prod_{j=1}^{n} \left[\cos\left(\frac{\omega_0 \tau}{2}\right) \cos\left(\frac{\omega_1 \tau}{2}\right) + (\vec{n_0} \cdot \vec{n_1}) \sin\left(\frac{\omega_0 \tau}{2}\right) \sin\left(\frac{\omega_1 \tau}{2}\right) \right]^{(j)}. \quad (2)$$

We note that the expressions do not account for any relaxation processes. The Ramsey sequence is sensitive to detuning since the electron spin is not refocused and it decays with the electron spin T_2^*; however, it is possible to sense nuclear spins with vanishing perpendicular hyperfine coupling.

To extend the relaxation time and access more nuclei, one can insert a π pulse in the Ramsey sequence, creating a Hahn echo sequence, and obtain the following signal:

$$\langle \sigma_z \rangle_{\mathrm{HE}} = \prod_{j=1}^{n} \left[1 - 2k^2 \sin^2\left(\frac{\omega_0 \tau}{2}\right) \sin^2\left(\frac{\omega_1 \tau}{2}\right) \right]^{(j)}, \quad (3)$$

where $k = \frac{(s_1 - s_0)\omega_L A_{zx}}{\omega_0 \omega_1}$ is the modulation amplitude of each nuclear spin. Without any nuclear spin, the Hahn echo sequence creates an electron spin echo signal with an envelope of stretched exponential decay with T_2^{HE}. However, in the presence of nuclear spins, the electron spin echo envelope will be modulated due to interaction with the nuclei. Hence, this sequence is also called electron spin echo envelope modulation. Even though the coherence time is increased, distinguishing the effects of different nuclear spins in the total signal is very complicated. The Hahn echo sequence can be used for defects that contain a few strongly coupled nuclei. In order to differentiate the resonance frequency of each nuclear spin or to sharpen the oscillations, one can add more π pulses, creating the so-called dynamical decoupling (DD) sequence to separate the resonance conditions for individual nuclear spins. For an even number of π pulses N, the DD signal can be obtained (neglecting decoherence terms) as

$$\langle \sigma_z \rangle_{\mathrm{DD}} = \prod_{j=1}^{n} \left[1 - 2k^2 \sin^2\left(\frac{\omega_0 \tau}{2}\right) \sin^2\left(\frac{\omega_1 \tau}{2}\right) \frac{\sin^2\left(\frac{N}{2}\theta\right)}{\cos^2\left(\frac{1}{2}\theta\right)} \right]^{(j)}, \quad (4)$$

where

$$\theta = \arccos[\cos(\omega_0 \tau)\cos(\omega_1 \tau) - \vec{n}_0 \cdot \vec{n}_1 \sin(\omega_0 \tau)\sin(\omega_1 \tau)], \quad (5)$$

where $\vec{n}_0 \cdot \vec{n}_1 = \frac{\omega_L^2 + (s_0 + s_1)A_{zz} + s_0 s_1 (A_{zz}^2 + A_{zx}^2)}{\omega_0 \omega_1}$, which is the inner product of the precession axes of a nuclear spin condition on the electron spin sublevel. This expression indicates the advantage of using the DD sequence for sublevels where either s_0 or s_1 is zero: only first-order parallel hyperfine coupling $\frac{A_{zz}}{\omega_L}$ plays a role. On the other hand, in spin-1/2 systems ($s_0 = -\frac{1}{2}$ and $s_1 = \frac{1}{2}$), the first-order perturbation correction with respect to hyperfine coupling vanishes, and only second-order perturbation term with respect to parallel $(\frac{A_{zz}}{\omega_L})^2$ and perpendicular coupling $(\frac{A_{zx}}{\omega_L})^2$ remains present. This indicates weak sensitivity of the DD sequence to different nuclear spins. At this point, it should be clear that the number of pulses can be used as an additional parameter to modify the modulation depth of each nuclear spin. A detailed investigation of the obtained DD signal reveals that by sweeping the time interval between pulses, an exponential decay with a rate of $1/T_2$ is observed, except for some resonance times when the electron spin becomes entangled with a particular nuclear spin, resulting in a sharp drop in the signal. This resonance time can be obtained assuming $\omega_L \gg A_{zz}, A_{zx}$ is satisfied:

$$\tau_p \approx \frac{(2p+1)\pi}{\omega_0 + \omega_1} \approx \frac{(2p+1)\pi}{2\omega_L \left(1 + \frac{s_0 + s_1}{2}\frac{A_{zz}}{\omega_L} + \frac{s_0^2 + s_1^2}{4}\frac{A_{zx}^2}{\omega_L^2}\right)}. \quad (6)$$

Experimental observation of the resonance times provides valuable information about the nuclear spins. For instance, in the case of an NV center, the second-order term $\frac{A_{zx}^2}{\omega_L^2}$ can be neglected, allowing for the direct determination of the A_{zz} hyperfine component from the resonances. To proceed with the characterization, Eq. (4) needs to be further simplified, requiring stronger assumptions. Focusing on weakly coupled nuclear spins or high magnetic fields, the multiplication over all nuclear spins in Eq. (4) can be approximated by a summation rule, neglecting the higher-order cross-resonance terms:

$$\langle \sigma_z \rangle_{\mathrm{DD}} \approx 1 - 2 \sum_{j=1}^{n} \left[k^2 \sin^2\left(\frac{\omega_0 \tau}{2}\right) \sin^2\left(\frac{\omega_1 \tau}{2}\right) \frac{\sin^2\left(\frac{N}{2}\theta\right)}{\cos^2\left(\frac{1}{2}\theta\right)} \right]^{(j)}. \quad (7)$$

Assuming nonoverlapping resonance times (which does not hold true for spin-1/2 systems) and expanding the signal around the jth nuclear spin resonance ($\tau = \tau_p^{(j)} + \delta\tau$) up to the first order of $\delta\tau$ result in the ability to approximate each drop with a Lorentzian function:

$$\langle \sigma_z \rangle_{\mathrm{DD}}(\delta\tau) \approx 1 - 2\sin^2\left(\frac{N}{2}\frac{(s_1 - s_0)A_{zx}}{\omega_L}\right) \frac{\left(\frac{(s_1 - s_0)A_{zx}}{2\omega_L^2}\right)^2}{\delta\tau^2 + \left(\frac{(s_1 - s_0)A_{zx}}{2\omega_L^2}\right)^2}. \quad (8)$$

This simplification allows for the determination of the parallel component of the hyperfine interaction for each nuclear spin, possibly in two ways. First, a Lorentzian with a width of $\frac{(s_1 - s_0)A_{zx}}{\omega_L^2}$ can be fitted to a dip to identify A_{zx}. Second, by keeping track of the minima of a dip while varying the number of pulses, the periodic function $1 - 2\sin^2(\frac{N}{2}\frac{(s_1 - s_0)A_{zx}}{\omega_L})$ can be fitted to obtain A_{zx}.

Although the DD sequence is well understood and used to characterize nuclear spins, it is not applicable to all systems.

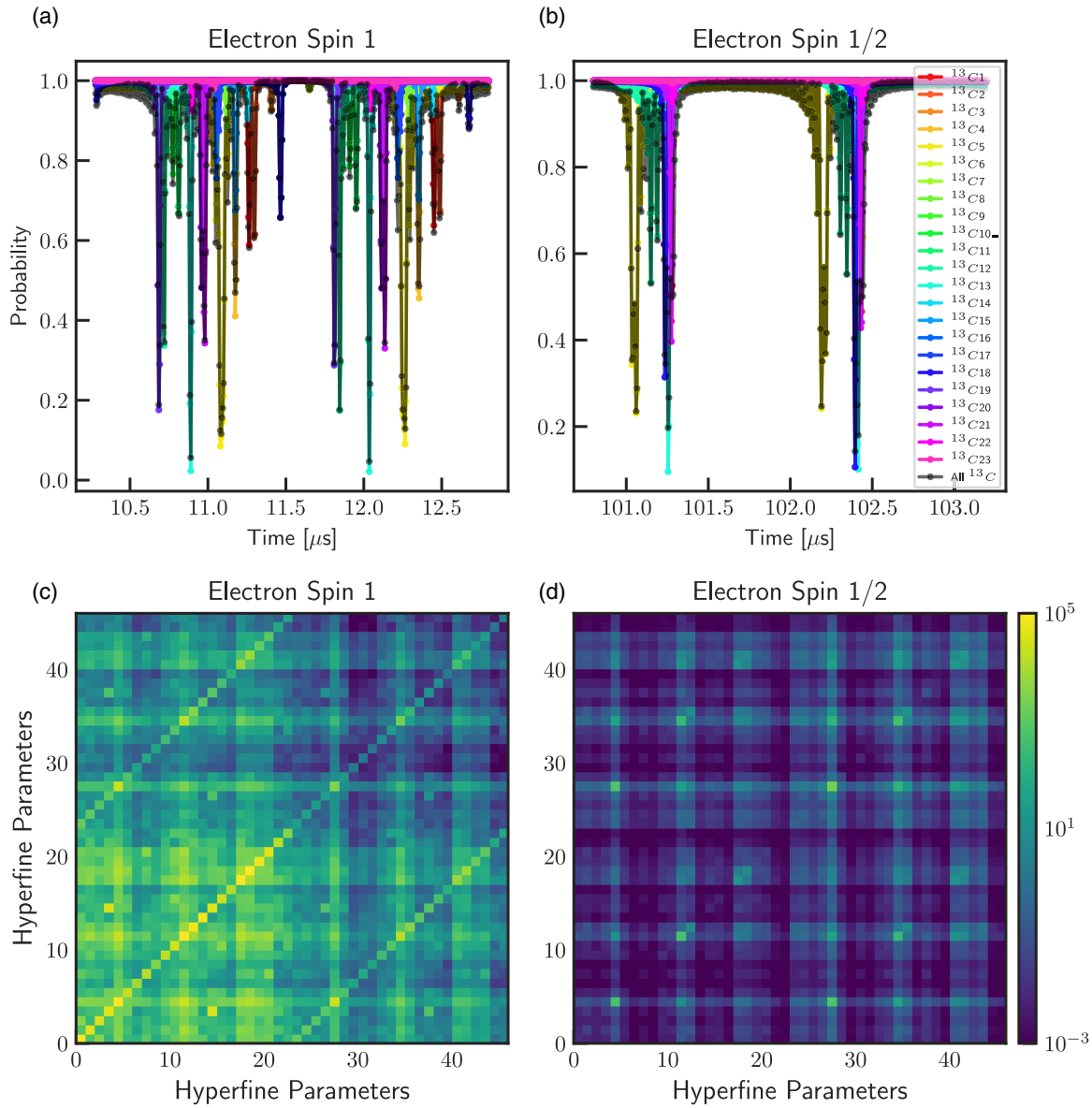

FIG. 2. Simulated DD signal with 64 π pulses for the register reported in [12] consisting of 23 nuclear spins, assuming the electron spin is (a) a spin $S = 1$ system and (b) a spin $S = 1/2$ system. Simulated Fisher information matrix for the case of the electron spin for (c) a spin $S = 1$ system and (d) a spin $S = 1/2$ system. The first 23 hyperfine parameters are A_{zz}, and the second 23 parameters are A_{zx} from the nuclear spin register.

First, DD works only for defects in high magnetic fields with weak hyperfine coupling ($\omega_L \gg A_{zz}, A_{zx}$). Second, the signal is limited to the electron spin T_2, which only gradually approaches T_1. Third, signal analysis is rather complicated and time-consuming; one has to collect enough data to ensure that no two nuclear spins overlap in the signal. Fourth, this sequence does not work for spin-1/2 systems, such as group IV defects in diamond, since the parallel component of the hyperfine coupling cancels their effect on the first-order electron spin signal. Hence, the resonance signal depends on the second order of the perpendicular hyperfine component.

In this work, we consider the 23-nuclear spin cluster characterized previously in [12] as a realistic case for our comparison. Each nuclear spin is identified by two hyperfine parameters, A_{zz} and A_{zx}, which show coupling to the central electron spin. Hence, characterizing these 23 nuclear spins requires identifying 56 hyperfine coupling parameters. First, we apply the DD sequence to this nuclear spin register and visualize the obtained results. Figure 2 compares the DD signal for the same nuclear spin register but different defects in diamond. An intuitive description of the sensitivity of a sequence to the variation of hyperfine coupling can be estimated by considering the width and sensitivity of the position of the resonances. First, we consider the case of an NV center in diamond. The width of a dip is $\delta\tau = \frac{A_{zx}}{\omega_L^2}$. Taking the derivative of the resonance time, we define the sensitivity of the longitudinal hyperfine coupling, using Eq. (6) to simplify it:

$$\delta A_{zz} \equiv \frac{\delta\tau}{\left|\frac{\partial\tau_p}{\partial A_{zz}}\right|} = \frac{2}{\tau_p}\frac{A_{zx}}{\omega_L} \geqslant \frac{4}{T_2^{\mathrm{HE}}}\frac{A_{zx}}{\omega_L}. \tag{9}$$

If we assume typical values of $T_2^{\mathrm{HE}} = 100$ μs and $\omega_L = 500$ kHz, a weakly coupled nuclear spin $A_{zx} = 5$ kHz can be distinguished from another weakly coupled nuclear spin with $\delta A_{zz} = 400$ Hz. For $S = 1/2$, like in group IV defects in diamond, the resonance times are sensitive to the second order of A_{zx} and show no sensitivity to A_{zz}. Hence, even at large τ, the resonances related to nuclear spins will not be well separated. We define the sensitivity of the spin-1/2 system as follows:

$$\delta A_{zx} \equiv \frac{\delta\tau}{\left|\frac{\partial\tau_k}{\partial A_{zx}}\right|} = \frac{4}{\tau_k} \geqslant \frac{8}{T_2^{\mathrm{HE}}}. \tag{10}$$

Assuming typical values of $T_2^{\mathrm{HE}} = 100$ μs, a nuclear spin can be distinguished from another one if their transverse hyperfine coupling is separated by $\delta A_{zx} = 80$ kHz, which is quite inaccurate and approximately 160 times worse than for $S = 1$.

To quantify the difference in sensitivity for estimating the hyperfine parameters, we perform calculations of the Fisher information matrix for the 23-nuclear-spin cluster, with 23 A_{zz} and 23 A_{zx} parameters [see Figs. 2(c) and 2(d)]. The Fisher information matrix is estimated for the probability to measure state $|0\rangle$ and reads

$$F_{ij}(\mathbf{A}) = \sum_{\tau} \frac{\partial p(0,\tau,\mathbf{A})}{\partial A_i} \frac{\partial p(0,\tau,\mathbf{A})}{\partial A_j} \frac{1}{p(1-p)}. \tag{11}$$

The summation is over τ, the pulse timing used in the sequence, and A is the array including all hyperfine coupling parameters. For the considered nuclear spin register, A includes 56 hyperfine coupling parameters; the first 23 parameters are A_{zz} of different nuclear spins, and the second 23 parameters are A_{zx}, resulting in the Fisher information being a 56×56 matrix. Figures 2(c) and 2(d) visualize the Fisher information matrix element for the DD sequence in spin-1 and -1/2 systems. For the typical case of an NV center with $S = 1$, since all the nuclear spin resonances are clearly resolved, the Fisher information matrix takes a diagonal shape, revealing low covariances between the various nuclear spin resonances. There is cross talk between A_{zz} and A_{zx} for a nuclear spin, as the position of the peak depends on both values. The Fisher information provides a bound for the precision of parameter estimation, known as the Cramér-Rao bound:

$$\delta A^2 \geqslant \frac{1}{N} F(A)^{-1}. \tag{12}$$

=10 The striking difference from the $S = 1$ Fisher information matrix is the behavior of the defect with $S = 1/2$. First of all, for both spin $S = 1/2$ and $S = 1$, the sequence's spectral resolution is limited by the T_1 relaxation time of the electron spin. On the other hand, the sequence's sensitivity is limited by T_2. The main principle of five-pulse ESEEM [22] is to create entanglement (via, e.g., a Hahn echo or Carr-Purcell-Meiboom-Gill (CPMG) block) before the free evolution of the nuclear spins and then to apply a second correlating sequence afterwards. In other words, the initial density matrix for the Hahn echo sequence is modified so that entanglement already exists in the electron polarization terms of the density matrix, thus limited by time T_1. Figure 6 shows the sequence, which can be interpreted as two Hahn echoes separated by a long free evolution $T \gg T_2^*$ such that the coherence of the electron spin vanishes. The analytical formula for this sequence is provided in Appendix C. During the free evolution time, each nuclear spin oscillates with one of two resonance frequencies obtained from Eq. (1).

Figure 3 shows the Fourier transform of the signal. Zooming into the area close to the Larmor frequency reveals the weakly coupled nuclei. Each nuclear spin has two peaks in the spectrum, ω_a and ω_b. Expanding the resonance frequencies up to first order with respect to hyperfine coupling shows that nuclear spins appear in order of their coupling strength, making their characterization rather straightforward. To observe the weakly coupled nuclei more clearly, one can use the DD-ESEEM sequence by adding more π pulses in the entangling periods. To distinguish other nuclei, extra measurements are required. One method is to use two-dimensional hyperfine correlation spectroscopy (2D HYperfine Sublevel CORrelation sequence (Hyscore)) [17]. However, this method is rather time-consuming because two time variables have to be swept. Optimum time sampling techniques might be used to optimize the timing of 2D sampling. Here, we suggest an alternative method which is conventionally used in electron spin resonance, i.e., sweeping the τ parameter and keeping track of the frequency amplitude as a function of τ. Two frequencies that belong to the same nucleus are correlated because the modulation depth oscillates with blind spot terms of both frequencies $\sin^2(\frac{\omega_0\tau}{2})\sin^2(\frac{\omega_1\tau}{2})$. Figure 4 shows two frequencies going to bright and blind spots simultaneously. Hence, by taking a two-dimensional correlation of the spectrum, one can deduce which two frequencies are correlated and belong to the same nucleus.

To simulate a realistic experimental situation, we model the electron spin state as projected to 0 and 1 with a binomial distribution where the probability is determined by analytical expressions. Then, we assume the bright (dark) state emits 3 (0.1) photons on average with a Poissonian distribution. We repeat the measurement at each point 10 000 times to reduce classical photon shot noise.

To estimate the number of nuclear spins that can be identified, we consider the duration of the free evolution time and the choice of interpulse timing τ. For a realistic scenario with $T_1 = 1$ s and $T_2 = 100$ μs, sweeping the relevant parameter in 1000 steps, we can estimate the Fisher information matrix for various protocols. We will approach the system with a moderate number of pulses, say, $N = 16$, for the dynamical decoupling sequence and the simplest five-pulse ESEEM for the correlation protocol for simplicity of calculation, as analytical expressions are available in that case.

Figure 5 illustrates the manifestation of the correlation protocol for a spin-1/2 system in terms of the number of nuclear spins one can estimate with each of the protocols. The dots on the A_{zz} and A_{zx} axes represent the points, with an area bounded by the Cramér-Rao bound around each point. A nuclear spin is considered detectable (blue points in Fig. 5) if the uncertainty of one of the two hyperfine parameters is less than both the absolute value of that parameter and the distance to the closest hyperfine coupling. Otherwise, it is considered nonidentified (shown as red points). Additionally, covariance between various parameters is calculated from the off-diagonal elements in the inverse Fisher information matrix. To illustrate them, an ellipse for each covariance parameter is plotted (colored orange and pink), with two nuclei being the vertices of the ellipse and the small axis size being the Cramér-Rao bound.

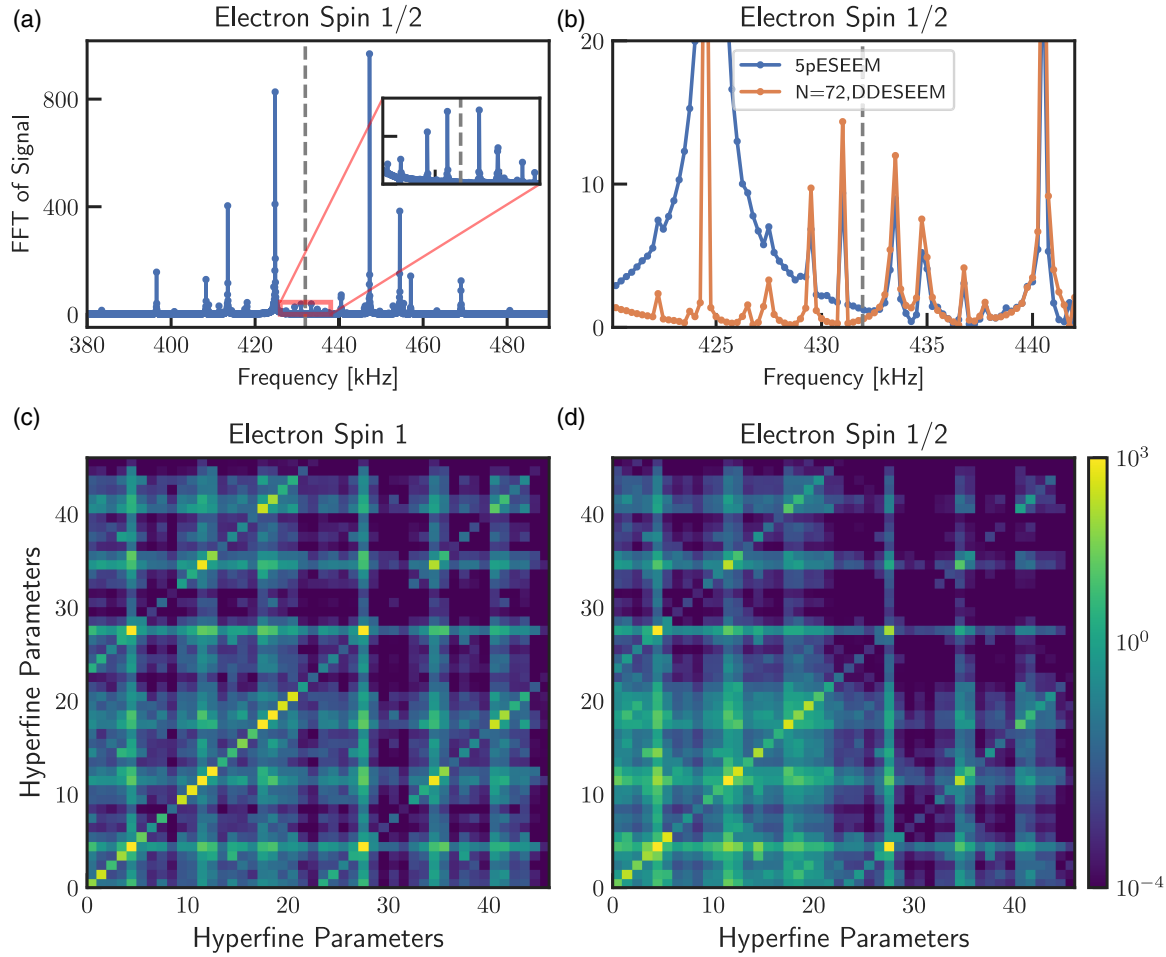

FIG. 3. (a) Simulated FFT of the ESEEM signal with a zoom into weakly coupled nuclear spins for the register reported in [12] consisting of 23 nuclear spins, assuming the electron spin $S = 1/2$ system. (b) Enhancing the sensitivity to weakly coupled spins by increasing the number of π pulses to $N = 72$ pulses in each entangling period. τ is set to the Larmor bright spot. Simulated five-pulse ESEEM Fisher information 56×56 matrix for the cases of the electron spin (c) $S = 1$ and (d) $S = 1/2$ systems. The first 23 hyperfine parameters are A_{zz}, and the second 23 parameters are A_{zx} from the nuclear spin register. It indicates the covariance between two parameters. The main diagonal appears because each parameter is correlated with itself. The side diagonals indicate the two hyperfine parameters that belong to the same nuclei.

This means that in the case of zero covariance between two nuclei, this ellipse turns into a line. To keep the plot readable, for each nuclear spin, only the ellipse with the largest covariance value is plotted. These covariances mostly show the cross talk between different parameters in the presented data and are more strongly present in the DD $S = 1/2$ case. The idea behind the ellipse representation is that when the covariance is larger than the self-variance, the spins become indistinguishable. While this cross talk is not the limiting factor of the informational approach, it might be important when considering a realistic estimator. It is important to note that this is not strictly the same condition as in experimental identification and is idealized. We consider only the available information in the plot, assuming that an optimum estimator

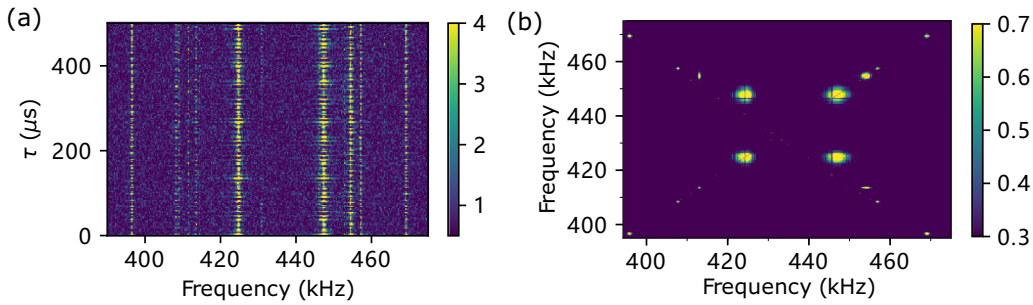

FIG. 4. (a) FFT of the ESEEM signal for τ from 10 to 500 μs with a step of 10 μs (b) Two-dimensional correlation of each frequency for different τ.

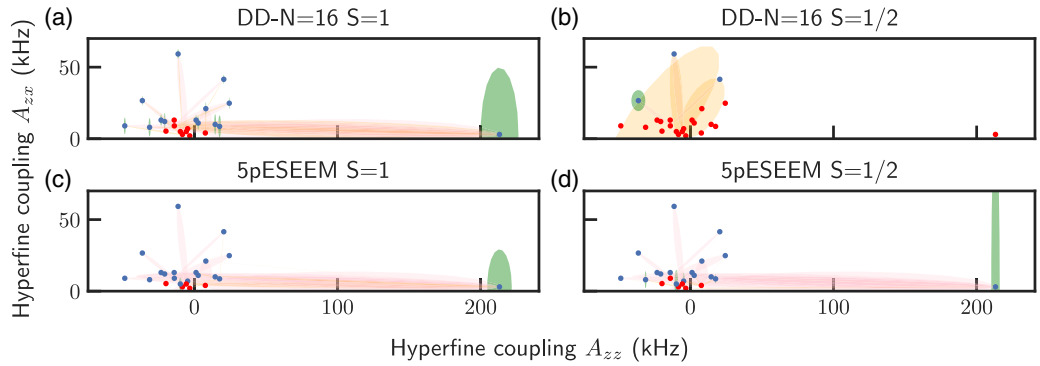

FIG. 5. Visualization of the Cramér-Rao bound for various protocols on an existing nuclear spin dataset from [12].

for the extraction of that information already exists. In reality, one has to additionally assume a nonideal estimator procedure, which involves the extraction of the hyperfine parameter values from the raw data. But that is a subject for future work. As a result, we see that while for the DD method a spin-1/2 case for $N = 16$ pulses allows for the identification of only 3 out of 23 nuclear spins, the five-pulse ESEEM method works with similar success for both $S = 1$ and $S = 1/2$ systems. In total, it is capable of detecting 17–18 out of 23 spins within the measurement time constraint. This could be further boosted by using the DD-ESEEM method with multiple pulses in each sensing block analogous to Fig. 3.

III. DISCUSSION

In this work, we conducted a theoretical and numerical comparison of various ESEEM methods for characterizing the nuclear spin clusters around $S = 1$ and $S = 1/2$ types of defects. We found that for $S = 1$ systems, modified spin echo sequences such as phase cycled CPMG (XY8) are most suited for single nuclear spin qubit spectroscopy, but for $S = 1/2$ systems, their performance is limited. On the other hand, correlation-type sequences like three- and five-pulse ESEEM show greater potential for characterizing a diluted nuclear spin bath and perform at least as well as in the $S = 1$ case. We believe that these methods hold significant potential for preliminary screening of nuclear spin clusters for $S = 1/2$ potential qubit candidate systems, such as G-IV defects in diamond. Additionally, our method does not require strong microwave pulse fields since the pulses do not need to cope with the nuclear spin Larmor frequency. While we explored various sensing methods in this work, we did not delve into estimator performance. We believe that this aspect should be considered in conjunction with adaptive and optimal strategies for controlling the experimental parameters, such as Bayesian optimal experimental design and machine learning, to increase the efficiency of estimation. This could further enhance the characterization capabilities of these methods in practical experimental scenarios.

ACKNOWLEDGMENTS

We acknowledge financial support from the European Union's Horizon 2020 research and innovation program ASTERIQS under Grant No. 820394, as well as Federal Ministry of Education and Research (BMBF) projects MiLiQuant and Quamapolis, Spinning and QR.X, the DFG (FOR 2724, INST 41/1109-1 FUGG), the Max Planck Society, and the Volkswagentiftung. M.Z. thanks the Max Planck School of Photonics for financial support.

APPENDIX A: SEQUENCES

The details of the sequences mentioned in the main text can be found in Fig. 6.

APPENDIX B: HAMILTONIAN

The spin Hamiltonian for many color centers can be written as [23]

$$H = \mathbf{D}^{\intercal}\mathbf{S}\mathbf{D} + \beta_e \mathbf{B}^{\intercal}\mathbf{g}\mathbf{S} + \beta_n \sum_{k=1}^{m} g_n^{(k)} \mathbf{B}^{\intercal}\mathbf{I}^{(k)} + \sum_{I_k > 1/2} (\mathbf{I}^{\intercal}\mathbf{P}\mathbf{I})^{(k)} + \sum_{k=1}^{m} g_n^{(k)} (\mathbf{S}^{\intercal}\mathbf{A}\mathbf{I})^{(k)}, \quad \text{(B1)}$$

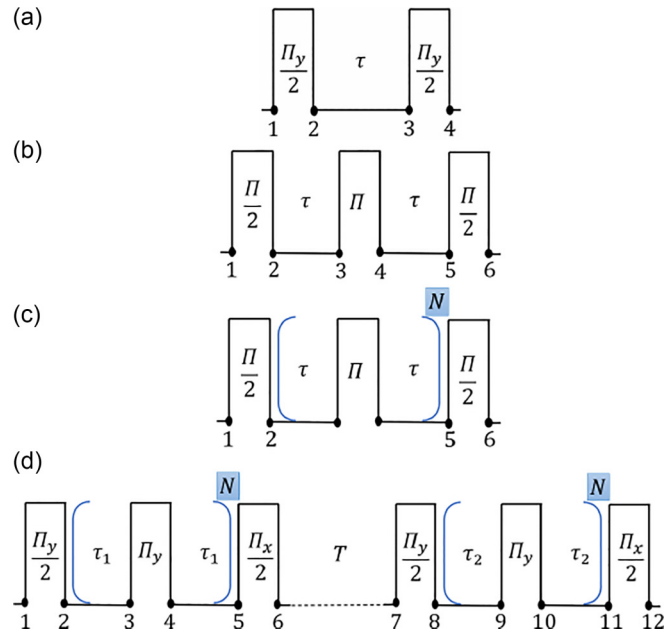

FIG. 6. Pulse sequences: (a) Ramsey, (b) Hahn echo, (c) dynamical decoupling, and (d) DDESEEM.

where $\mathbf{S}$ and $\mathbf{I}^{(k)}$ are electron and nuclear spin vector operators, $\mathbf{D}$ is the zero-field-splitting tensor, $\mathbf{B}$ is the magnetic field vector, $\mathbf{P}$ is the nuclear quadrupole tensor, $\mathbf{A}$ is the hyperfine interaction tensor, and $\beta_e = \frac{e\hbar}{2m_e}$ and $\beta_n = \frac{-e\hbar}{2m_n}$ are the electron and nuclear Bohr magnetons. Here, we neglected nuclear-nuclear interactions. Also, due to axial symmetry, the zero-field splitting can be simplified. We assume the magnetic field is only along the symmetry axis, which we denote as the z direction. Moreover, the secular terms (S_zI_x, S_zI_y, S_zI_z) are just a shift of the energy level that are relevant up to first order, while the nonsecular terms $(S_xI_x, S_yI_x, S_zI_z, S_xI_y, S_yI_y, S_zI_y)$ mix the electron spin levels, which are largely detuned due to the large zero-field splitting. Hence, the nonsecular terms of the Hamiltonian are neglected. Furthermore, for each nuclear spin, one can go to the xy frame such that the A_{zy} term is zero. All in all, the spin Hamiltonian with the mentioned considerations can be simplified to

$$H = D_zS_z^2 + \gamma_eBS_z + \gamma_nBI_z^{(k)} + P_z^{(k)}I_z^{2(k)} + A_{zz}^{(k)}S_zI_z^{(k)} + A_{zx}^{(k)}S_zI_x^{(k)}. \tag{B2}$$

The summation over k is omitted for convenience. The coefficients γ_e and γ_n are the electron and nuclear gyromagnetic ratios. The coefficients' values for the case of a NV center in diamond are $D_z = 2.87$ GHz, $\gamma_e = -2.802$ MHz/G, $\gamma_n^{(^{13}C)} = 1.07$ kHz/G, $\gamma_n^{(^{14}N)} = 0.31$ kHz/G, and $P_z^{(^{14}N)} = -5.04$ MHz.

The electron spin in general can take any value; however, resonant microwave pulses are applied only for two of the sublevels. Hence, the electron spin is effectively a two-level system. The electron spin occupies two of its sublevels, which are denoted as $|0\rangle = |m_s = s_0\rangle$ and $|1\rangle = |m_s = s_1\rangle$; in other words,

$$S_z = \begin{pmatrix} s_1 & 0 \\ 0 & s_0 \end{pmatrix}. \tag{B3}$$

One can show that $S_z^2 = (s_1 + s_0)S_z - s_1s_0\mathbb{1}$. We define the transition frequency between two spin sublevels of the electron spin as $\omega_a = D_z(s_1 + s_0) + \gamma_eB$. Moreover, we note that since we consider nuclei with a spin of $1/2$ in the system, the nuclear quadrupole term vanishes. The Hamiltonian can be written in terms of Pauli matrices:

$$H = \omega_aS_z + \gamma_nBI_z^{(k)} + A_{zz}^{(k)}S_zI_z^{(k)} + A_{zx}^{(k)}S_zI_x^{(k)}. \tag{B4}$$

The Hamiltonian presented so far does not include the microwave drive field. Indeed, the microwave pulses are assumed to be instantaneous, but considering the drive field, the Hamiltonian should be written in the rotating frame and assume the rotating wave approximation. This frame should be respected for the rest of the sequence. Since the rotating frame unitary operator commutes with σ_z, the expectation value of this operator in the rotating frame is the same as in the laboratory frame. Eventually, the free evolution Hamiltonian in the rotating frame is written as follows:

$$H = \Delta S_z + \sum_k \left(\omega_L^{(k)} + A_{zz}^{(k)}S_z\right)I_z^{(k)} + A_{zx}^{(k)}S_zI_x^{(k)}, \tag{B5}$$

where $\Delta = \omega_a - \omega_{mw}$ is the detuning.

APPENDIX C: FIVE-PULSE ESEEM FORMULA

To define the unitary operators, let us introduce three sets of operators representing the evolution during the sequence: (1) The evolution during the first Hahn echo is given by the V operators. (2) The middle free evolution is represented by the F operators. (3) The second Hahn echo is governed by the W operators:

$$V_0 = U_0(\tau_1)U_1(\tau_1),\ V_1 = U_1(\tau_1)U_0(\tau_1), \tag{C1}$$

$$F_0 = U_0(T),\ F_1 = U_1(T)U_0, \tag{C2}$$

$$W_0 = U_0(\tau_2)U_1(\tau_2),\ W_1 = U_1(\tau_2)U_0(\tau_2). \tag{C3}$$

These operators define the trajectory of the electron spin during the five-pulse ESEEM sequence. The signal can be obtained from four different types of trajectories that the electron spin can take. We can express every unitary operator in terms of a rotation angle, axis, and Pauli matrices $\vec{\sigma}$. We denote the unitary operator U as $U = \exp(-i\theta_U\hat{n}_U \cdot \vec{\sigma}) = M\cos(\theta_U)\mathbf{I} - i\sin(\theta_U)\hat{n}_U \cdot \vec{\sigma}$. The signal for five-pulse ESEEM can be obtained as follows:

$$\begin{aligned}\langle\sigma_z\rangle_{5p} = \frac{1}{4}\Bigg\{ &\prod_{j=1}^{n}\left[\cos\left(\theta_{W_1F_1V_0V_1^\dagger F_1^\dagger W_0^\dagger}\right)\right]^{(j)} \\ &- \prod_{j=1}^{n}\left[\cos\left(\theta_{W_1F_1V_1V_0^\dagger F_1^\dagger W_0^\dagger}\right)\right]^{(j)} \\ &+ \prod_{j=1}^{n}\left[\cos\left(\theta_{W_1F_0V_0V_1^\dagger F_0^\dagger W_0^\dagger}\right)\right]^{(j)} \\ &- \prod_{j=1}^{n}\left[\cos\left(\theta_{W_1F_0V_1V_0^\dagger F_0^\dagger W_0^\dagger}\right)\right]^{(j)}\Bigg\}.\end{aligned} \tag{C4}$$

Multiplying the matrices and finding the rotation angles give an expectation value of σ_z for the five-pulse ESEEM sequence as it can be found in this article [22]:

$$\langle\sigma_z\rangle_{5p} = \frac{1}{4}\left(\prod_{j=1}^{n}E_{\alpha_+}^{(j)} - \prod_{j=1}^{n}E_{\alpha_-}^{(j)} + \prod_{j=1}^{n}E_{\beta_+}^{(j)} - \prod_{j=1}^{n}E_{\beta_-}^{(j)}\right), \tag{C5}$$

where each term can be calculated as follows:

$$\begin{aligned}E_{\alpha_\pm}^{(k)} = &E_{2p}(\tau_1)E_{2p}(\tau_2) \mp B[-4k^2C_\alpha \\ &+ 4k\cos^4(\eta)\cos(\omega_\alpha T + \phi_{\alpha_+} + \phi_{\beta_+}) \\ &+ 2k^2\cos(\phi_{\beta_-})\cos(\omega_\alpha T + \phi_{\alpha_+}) \\ &+ 4k\sin^4(\eta)\cos(\omega_\alpha T + \phi_{\alpha_+} - \phi_{\beta_+})].\end{aligned} \tag{C6}$$

E_{2p} is a two-pulse ESEEM sequence signal:

$$\begin{aligned}E_{2p}(t) = &\left(1 - \frac{k}{2}\right) + \frac{k}{2}\Big[\cos(\omega_\alpha t) + \cos(\omega_\beta t) \\ &- \frac{1}{2}\cos(\omega_- t) - \frac{1}{2}\cos(\omega_+ t)\Big],\end{aligned} \tag{C7}$$

where $\omega_{\pm} = \omega_{\alpha} \pm \omega_{\beta}$, B is the blind spot term, and C_{α} is a constant term:

$$B = \sin\left(\frac{\omega_{\alpha}\tau_1}{2}\right)\sin\left(\frac{\omega_{\alpha}\tau_2}{2}\right)\sin\left(\frac{\omega_{\beta}\tau_1}{2}\right)\sin\left(\frac{\omega_{\beta}\tau_2}{2}\right), \tag{C8}$$

$$C_{\alpha} = \cos\left(\frac{\omega_{\alpha}\tau_1}{2}\right)\cos\left(\frac{\omega_{\alpha}\tau_2}{2}\right)\sin\left(\frac{\omega_{\beta}\tau_1}{2}\right)\sin\left(\frac{\omega_{\beta}\tau_2}{2}\right). \tag{C9}$$

The resonance frequencies are $\omega_{\alpha(\beta)} = \sqrt{(\omega_L + s_{0(1)}A_{zz})^2 + (s_{0(1)}A_{zx})^2}$. The quantization axis of nuclear spins is tilted by $\eta_{\alpha(\beta)} = \arctan(\frac{s_{0(1)}A_{zx}}{\omega_L + s_{0(1)}A_{zz}})$, which gives the parameter $\eta = \frac{\eta_{\alpha} - \eta_{\beta}}{2}$. The modulation depth of each nuclear spin is $k = \sin^2(2\eta) = (\frac{(s_1 - s_0)\omega_L A_{zx}}{\omega_{\alpha}\omega_{\beta}})^2$, and the phase shifts are $\phi_{\alpha_{\pm}} = \frac{\omega_{\alpha}(\tau_1 \pm \tau_2)}{2}$ and $\phi_{\beta_{\pm}} = \frac{\omega_{\beta}(\tau_1 \pm \tau_2)}{2}$. The two expression for the β pathways can be obtained by exchanging α and β in Eqs. (C6), (C8), and (C9).

As demonstrated, the signal from the nuclear spin register arises from the multiplication of signals from individual nuclear spins. Consequently, if the modulation depth is not low (indicative of low magnetic field conditions), higher-order frequencies will manifest in the spectrum. Thus, the product rule gives rise to internuclear peaks at multiquantum frequencies, which can represent sums or subtractions of single quantum frequencies from various nuclei. However, these multiple quantum resonance peaks are informative for electron spin-1/2 systems because they enable the deduction that two peaks added or subtracted belong to the same electron spin manifold, allowing for the determination of the relative phase of the nuclei. Another consequence of the product rule is the cross-suppression effect, in which the presence of strongly coupled nuclei suppresses the amplitude of weakly coupled nuclei, while weakly coupled ones do not suppress the amplitude of strongly coupled nuclei [24]. However, assuming a relatively high Larmor frequency or low modulation depth, both of these effects will vanish because the product rule can be approximated by a summation rule:

$$\begin{aligned} E_{\alpha} &= \prod_{j=1}^{n} E_{\alpha_+}^{(j)} - \prod_{j=1}^{n} E_{\alpha_-}^{(j)} \\ &\approx \sum_{j=1}^{n} [-8Bk\cos^4(\eta)\cos(\omega_{\alpha}T + \phi_{\alpha_+} + \phi_{\beta_+})]^{(j)}. \end{aligned} \tag{C10}$$

The blind spot term B shows how this sequence can be engineered to increase or reduce the signal amplitude of one nuclear spin from the spectrum. Equation (C8) suggests the bright and blind spots of a frequency can be obtained as follows:

$$\tau = \text{even}\ \frac{\pi}{\omega} \tag{C11}$$

for blind spots and

$$\tau = \text{odd}\ \frac{\pi}{\omega} \tag{C12}$$

for bright spots. The blind spot term depends on both τ_1 and τ_2. This means that if one resonant frequency is blinded, the other resonant frequency and all the multiple quantum resonances also vanish. This can be used as an indication of which two peaks in the frequency spectrum originate from the same nuclei. In other words, if one chooses a τ such that a particular resonant frequency in the spectrum is blinded, the other resonant frequency of the same nuclear spin will also be blinded, and both of them disappear from the frequency spectrum together. Moreover, this is especially helpful in the presence of strongly coupled nuclear spins that suppress other nuclei. By sweeping τ_1 and τ_2, one can go through different bright and blind spots of each nuclear spin and observe the correlations between different peaks.

APPENDIX D: DD ANALYSIS FOR BISPECIES SYSTEMS

Consider a single color center that is surrounded by two nuclear spin species. Each species has a distinct bath which is processed with its corresponding Larmor frequency. Assuming large Larmor frequency with respect to hyperfine couplings, one can write Eq. (7) for two baths ($\omega_0 \approx \omega_1 \approx \omega_L$) as follows:

$$\langle\sigma_z\rangle_{\text{bath}} \approx 1 - 2k_1^2\sin^4\left(\frac{\omega_L^{(1)}\tau}{2}\right) - 2k_2^2\sin^4\left(\frac{\omega_L^{(2)}\tau}{2}\right). \tag{D1}$$

This means that two baths interfere, and the periodicity of the total bath is not straightforward anymore. Hence, if there is a narrow peak next in the DD signal, it can be attributed to both of the baths. To clarify the type of nuclear spins, one has to perform further experiments, e.g., in various external magnetic fields.

[1] D. D. Awschalom, R. Hanson, J. Wrachtrup, and B. B. Zhou, Quantum technologies with optically interfaced solid-state spins, Nat. Photon. **12**, 516 (2018).

[2] M. Pompili *et al.*, Realization of a multinode quantum network of remote solid-state qubits, Science **372**, 259 (2021).

[3] C. L. Degen, F. Reinhard, and P. Cappellaro, Quantum sensing, Rev. Mod. Phys. **89**, 035002 (2017).

[4] J. Meinel, M. Kwon, R. Maier, D. Dasari, H. Sumiya, S. Onoda, J. Isoya, V. Vorobyov, and J. Wrachtrup, High-resolution nanoscale NMR for arbitrary magnetic fields, Commun. Phys. **6**, 302 (2023).

[5] C. E. Bradley, J. Randall, M. H. Abobeih, R. C. Berrevoets, M. J. Degen, M. A. Bakker, M. Markham, D. J. Twitchen, and T. H. Taminiau, A ten-qubit solid-state spin register with quantum memory up to one minute, Phys. Rev. X **9**, 031045 (2019).

[6] V. Vorobyov, S. Zaiser, N. Abt, J. Meinel, D. Dasari, P. Neumann, and J. Wrachtrup, Quantum fourier transform for nanoscale quantum sensing, npj Quantum Inf. **7**, 124 (2021).

[7] E. Hesselmeier *et al.*, Qudit-based spectroscopy for measurement and control of nuclear-spin qubits in silicon carbide, Phys. Rev. Lett. **132**, 090601 (2024).

[8] E. Hesselmeier, P. Kuna, W. Knolle, F. Kaiser, N. T. Son, M. Ghezellou, J. Ul-Hassan, V. Vorobyov, and J. Wrachtrup, High-fidelity optical readout of a nuclear-spin qubit in silicon carbide, Phys. Rev. Lett. **132**, 180804 (2024).

[9] J. Reiner *et al.*, High-fidelity initialization and control of electron and nuclear spins in a four-qubit register, Nat. Nanotechnol. **19**, 605 (2024).

[10] V. V. Vorobyov, J. Meinel, H. Sumiya, S. Onoda, J. Isoya, O. Gulinsky, and J. Wrachtrup, Transition from quantum to classical dynamics in weak measurements and reconstruction of quantum correlation, Phys. Rev. A **107**, 042212 (2023).

[11] C. Bradley *et al.*, Robust quantum-network memory based on spin qubits in isotopically engineered diamond, npj Quantum Inf. **8**, 122 (2022).

[12] M. Abobeih, J. Randall, C. Bradley, H. Bartling, M. Bakker, M. Degen, M. Markham, D. Twitchen, and T. Taminiau, Atomic-scale imaging of a 27-nuclear-spin cluster using a quantum sensor, Nature (London) **576**, 411 (2019).

[13] G. L. van de Stolpe, D. Kwiatkowski, C. Bradley, J. Randall, M. Abobeih, S. Breitweiser, L. Bassett, M. Markham, D. Twitchen, and T. Taminiau, Mapping a 50-spin-qubit network through correlated sensing, Nat. Commun. **15**, 2006 (2024).

[14] A. Dréau, J.-R. Maze, M. Lesik, J.-F. Roch, and V. Jacques, High-resolution spectroscopy of single NV defects coupled with nearby ^{13}C nuclear spins in diamond, Phys. Rev. B **85**, 134107 (2012).

[15] L. Childress, M. Gurudev Dutt, J. Taylor, A. Zibrov, F. Jelezko, J. Wrachtrup, P. Hemmer, and M. Lukin, Coherent dynamics of coupled electron and nuclear spin qubits in diamond, Science **314**, 281 (2006).

[16] A. Laraoui, F. Dolde, C. Burk, F. Reinhard, J. Wrachtrup, and C. A. Meriles, High-resolution correlation spectroscopy of ^{13}C spins near a nitrogen-vacancy centre in diamond, Nat. Commun. **4**, 1651 (2013).

[17] V. Vorobyov, J. Javadzade, M. Joliffe, F. Kaiser, and J. Wrachtrup, Addressing single nuclear spins quantum memories by a central electron spin, Appl. Magn. Reson. **53**, 1317 (2022).

[18] T. H. Taminiau, J. J. T. Wagenaar, T. van der Sar, F. Jelezko, V. V. Dobrovitski, and R. Hanson, Detection and control of individual nuclear spins using a weakly coupled electron spin, Phys. Rev. Lett. **109**, 137602 (2012).

[19] N. Zhao, J. Wrachtrup, and R.-B. Liu, Dynamical decoupling design for identifying weakly coupled nuclear spins in a bath, Phys. Rev. A **90**, 032319 (2014).

[20] P. Neumann, J. Beck, M. Steiner, F. Rempp, H. Fedder, P. R. Hemmer, J. Wrachtrup, and F. Jelezko, Single-shot readout of a single nuclear spin, Science **329**, 542 (2010).

[21] S. Zaiser, T. Rendler, I. Jakobi, T. Wolf, S.-Y. Lee, S. Wagner, V. Bergholm, T. Schulte-Herbrüggen, P. Neumann, and J. Wrachtrup, Enhancing quantum sensing sensitivity by a quantum memory, Nat. Commun. **7**, 12279 (2016).

[22] B. Kasumaj and S. Stoll, 5-and 6-pulse electron spin echo envelope modulation (ESEEM) of multi-nuclear spin systems, J. Magn. Reson. **190**, 233 (2008).

[23] A. Schweiger and G. Jeschke, *Principles of Pulse Electron Paramagnetic Resonance* (Oxford University Press, Oxford, 2001).

[24] S. Stoll, C. Calle, G. Mitrikas, and A. Schweiger, Peak suppression in ESEEM spectra of multinuclear spin systems, J. Magn. Reson. **177**, 93 (2005).